Ink - based non-vacuum process of synthesis of multicomponent $Cu_2ZnSn(Se_{1-x},S_x)_4$ for use in low-cost photovoltaic absorbers

Shailesh Narain Sharma[1]*, Parul Chawla[1], Shefali Jain[1], Mansoor Ahamed[1,2], N. Vijayan[1], J. Sharma[1]

[1]*Network of Institutes for Solar Energy, CSIR-National Physical Laboratory, Dr. K.S. Krishnan Marg, New Delhi, 110012, India*
[2]*Amity Institute of Nanotechnology, Amity University, Noida, UP, 201313, India*

*Corresponding author, Tel: (+91)1145609193; E-mail: shailesh@mail.nplindia.org

Received: 10 April 2016, Revised: 08 August 2016 and Accepted: 12 August 2016

DOI: 10.5185/amp.2016/202
www.vbripress.com/amp

Abstract

In this present work, $Cu_2ZnSn(Se_{1-x},S_x)_4$ nanocrystals with tunable band gaps have been synthesized via hot injection method in conjunction with TOP/TOP capping ligands. By varying the input precursor ratio Se/(S + Se), by adjusting the composition parameter x from 0 to 1.0, the band gaps of the CZTSSe-based nanocrystals can be linearly tuned from 1.2 to 1.5 eV respectively. For CZTSSe-based nanocrystals, high intensity of XRD peak corresponding to (112) direction revealed that the growth is oriented along (112) direction and its intensity increases with increase in Se/(S + Se) input precursor ratio. As the Se-content increases, the larger Se atoms (1.98 Å) replace the smaller larger S atoms (1.84 Å) resulting in an increase in the lattice parameters as shown by the shift of the XRD peaks to lower values of 2θ.XRD studies reveal the presence of stable kesterite phase although the presence of either stannite phase or both cannot be ruled out completely. It has been found that CZTSSe nanocrystallites owing to its high crystallinity and well-ordered 3-dimensional network and hence controlled morphology in its pristine form as compared with CZTSe, CZTS counterparts exhibits higher homogeneity, resistance against agglomeration and eventually higher current-voltage characteristics. To, the best of our knowledge, this is the first detailed report on the synthesis of multicomponent $Cu_2ZnSn(Se_{1-x},S_x)_4$ nanocrystals by hot injection method via the usage of both TOP (trioctyl phosphine) & TOPO (trioctyl phosphine oxide) capping ligands. The primary technological advantage of creating nanocrystals by this solution based method is the capability to easily form an ink that is compatible with a large variety of scalable film formation or printing processes for photovoltaic applications.

Keywords: CZTSSe-based inks, tunable band gap, non-vacuum process, TOPO/TOP capping ligands, photovoltaics.

Introduction

An ideal thin-film solar cell absorber material should have a direct band gap around 1.3–1.5 eV with abundant, inexpensive, and nontoxic elements. $Cu(InGa)Se_2$, (CIGS) is one of the most promising thin-film solar cell materials, demonstrating an efficiency greater than 20% [**1-3**]. However, In and Ga are expensive components, and the band gap is usually not optimal for high efficiency CIGS solar cells. Thin film of $Cu_2ZnSn(Se_{1-x}, S_x)_4$ (CZTSeS) for values of $0 \leq x \leq 1$ has attracted significant interest lately as alternative absorber layers in $Cu(In,Ga)(S,Se)_2$ (CIGS) thin film solar cells [**4-6**]. These compounds have drawn significant interest because they contain only abundant and nontoxic elements Cu, Zn, Sn, S, and Se. The band gap of $Cu_2ZnSn(Se_{1-x}, S_x)_4$(CZTSeS) has been reported to vary between 0.95eV (x=0) and 1.5eV (x=1) by changing the Se:S ratio [**4-6**]. The substitution of sulphur for selenium in the structure increases the band gap. Potentially this will enable tailoring of the band gap, both as a single bandgap material and as one in which the absorber layer band gap varies with depth, thus enabling higher collection efficiencies and lower recombination rates (as in the case of CIGS and CIGSeS) [**7**]. The recent approaches have been the usage of an appropriate SeS_2/Se weight ratio during the annealing process, through which the band gap grading was realized and consequently, CZTSSe solar cells with a maximum efficiency of 12.3% were obtained [**8**]. Recently, Khadka et al. [**9**] has found improvement in the crystal growth and device

properties of kesterite-based CZTSSe thin film solar cells upon alloying with Ge. Non-vacuum based processes are the cheapest and reliable means to obtain CZTSSe- based devices due to their numerous advantages over vacuum-based processes. These involve uniform and selective area deposition of the precursor materials which leads to high materials utilization thereby involving low capital investment for equipment which is approximately ~0.5$/W [**10**]. Non-vacuum processes involve the preparation of inks or slurries which can be deposited by spraying, printing, dip coating, or doctor blading [**10-12**]. In one approach, the metals are dissolved in acid and hydroxide nanoparticles are precipitated from this solution. The particles are dried, which results in a fine powder of mixed oxides. The powder is dispersed in an aqueous solution to obtain the ink. In this and similar processes the film composition can be controlled precisely and with relative ease by adjusting the relative amounts of material used for particle preparation. The oxide particle precursor needs an additional reduction step prior to selenization carried out in diluted hydrogen [**10-12**]. The precursor film can be porous because the volume increase during selenization leads to sufficient densification. Another approach involves the formation of precursor inks using colloidal approach by employing Schlenk line apparatus. This is an excellent procedure to produce a nanoparticle ink which can be effectively utilized as an absorber layer for the CZTSSe-based solar cell. However, developing a one-pot synthesis method to synthesize CZTSSe nanocrystals with controllable compositional values and tunable energy gap is still a demanding task due to the complexity in controlling both the phase purity and the composition [**13**]. CZTSSe nanocrystals with varying band gap from 1.0 to 1.5 eV using octadecene as a solvent cum ligand has been reported recently [**13**]. Till now, oleylamine (OLA) has been generally used for the colloidal synthesis of CZTSSe nanocrystals [**14**]. However, the high fabrication cost and the intricacy in ligand-exchange using OLA as the capping ligand calls for an alternative approach for the synthesis of CZTSSe nanocrystals. In this work, synthesis of CZTSSe-related inks have been done by colloidal route with various Se:S ratios, without resorting to post-synthesis selenization. TOPO(tri-n-octylphosphine oxide) and TOP(tri-n-octylphosphine) are two strong donor ligands that act as solvent-cum-capping agent during the synthesis of colloidal nanoparticles. The paper presents variations of bandgap value with Se:S ratio together with associated changes observed in the crystal structure and morphology. To the best of author's knowledge, non-vacuum based-synthesis of $Cu_2ZnSn(Se_{1-x}, S_x)_4$ (CZTSeS) compounds with TOPO/TOP capping ligands have been reported for the first time. Pure sulphides were also produced by direct sulphurisation of metallic precursors.

Experimental

Materials

(i) Copper (II) Chloride dihydrate ($CuCl_2.2H_2O$) (98% pure); (ii) Zinc(II) Chloride ($ZnCl_2$)(95% pure); (iii) Tin(IV) Chloride ($SnCl_4$) (98% pure); (iv) S & Se Powder (99.99% pure) & Capping Agents used: TOPO/TOP (97% pure). Above mentioned chemicals of analytical grade were procured from Sigma Aldrich were used without further purification.

Material synthesis

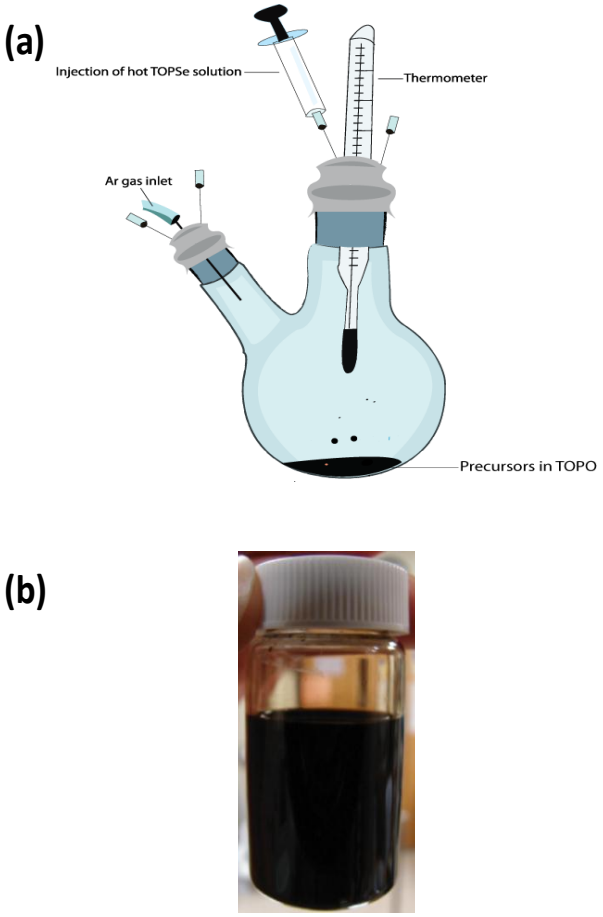

Fig. 1. (a) Schematics of the formation of CZTSSe-based nanoparticles in TOPO/TOP & (b) the purified CZTSSe-ink.

Colloidal CZTSSe-based nanoparticles were prepared by using the 'High temperature solid state injection' mechanism where one of the reactant dispersed in the solvent is injected into the other solvent-dispersed reactants at elevated temperatures. CZTSeS nanocrystals are synthesized by chemical-route using TOP (tri-octyl phosphine)/TOPO capping ligands. Here, hot injection of a solution of elemental selenium/sulphur in TOP into solution containing 1.5 mmol of copper(II) chloride, 0.75 mmol of zinc(II) chloride, 0.75 mmol of tin(IV) chloride in 2g TOPO at 275 °C takes place. All syntheses were carried out using a Schlenk line in an inert atmosphere of Ar as shown in **Fig. 1(a)**. A round two necked flask was

placed in a heating mantle with its two necks sealed with septum. A thermometer was inserted through the septum and into the mixture to provide accurate temperature control for the reaction. The highest temperature range used for the synthesis is 310-320^{0}C. Upon injection, the color changes from straw yellow to deep black. After the synthesis, the final solution was black and cooled down naturally with the heating mantle removed.

Purification Procedure

The prepared solution was then transferred to test tubes and 5 mL of anhydrous methanol was added to the mixture; this mixture was then centrifuged at 3000 rpm for 1 min. The clear supernatant was discarded and its precipitate was redispersed in 10 mL anhydrous toluene. A 5 mL portion of methanol was added to the solution and the nanoparticles were again isolated by centrifugation. After the supernatant was again decanted, the precipitates were redispersed in 8 mL of anhydrous toluene; the suspension was centrifuged at 3000 rpm for 1 min, yielding little sediment and a black coloured supernatant was obtained that was kept as the final product (**Fig. 1(b)**).

Characterization

TEM measurements were done by JEOL make model JEM-200CX with an acceleration potential of 200 kV. SEM micrographs were analyzed using Zeiss EVO MA-10 variable pressure SEM, samples being scanned at an accelerating voltage of 10.00 KV and WD of 12.00 mm at different magnifications from 1.00 KX - 30.00 KX under vacuum pressure of 10^{-6}torr. Powder X-ray diffraction (XRD) patterns (range 20°-80°) for the nanocrystals were recorded using a Bruker-AXS D8 advanced X-Ray diffractometer equipped with a Cu-Kα (λ=0.154 nm), X-ray source measured within the range (20° -80°) at the scanning speed of 0.01 deg/sec. Optical absorbance spectra of differently-capped nanocrystals dispersed in toluene was measured using a UV-3101 PC Shimadzu UV-Vis-NIR double-beam spectrophotometer.

Device Fabrications

The samples for I-V measurements have been spin-coated on-to the cleaned ITO-substrate by applying ~ 15 multiple coatings to obtain a thick film (~ 1 μm) particularly desirable for chalcogenide-based devices. This has been followed by the CdS buffer layer coating by using the chemical bath deposition process where the bath temperature has been maintained at ~ 85^{0}C for ~ 10 min for achieving the desirable thickness (~50-60 nm). To improve the contact between differently-capped nanocrystals and the CdS coating on each of them, a post-annealing has been done in an NEYTECH vacuum system at 200^{0}C for ~ 30 min using ramp rate of 10^{0}C/min. After all these procedures, the devices have been completed by vacuum-deposition of Al contacts using thermal evaporation unit where Al electrodes (100 nm) were deposited under reduced pressure of ~5 x10^{-6} mbar through shadow mask resulting in a device area of ~0.06 cm^2. The Current-Voltage (I-V) measurements were done using a Keithley Model 2420 High Current Source Meter unit (Keithley, USA) interfaced with computer.

Results and discussion

Importance of Capping -Ligand (TOPO/TOP)

TOPO ($CH_3(CH_2)_7]_3PO$) is a tertiary alkyl-phosphine that acts as a ligand in the synthesis procedure. TOP ($[CH_3(CH_2)_7]_3P$) is also one of the capping agent that is used in the synthesis of semiconductor nanoparticles.

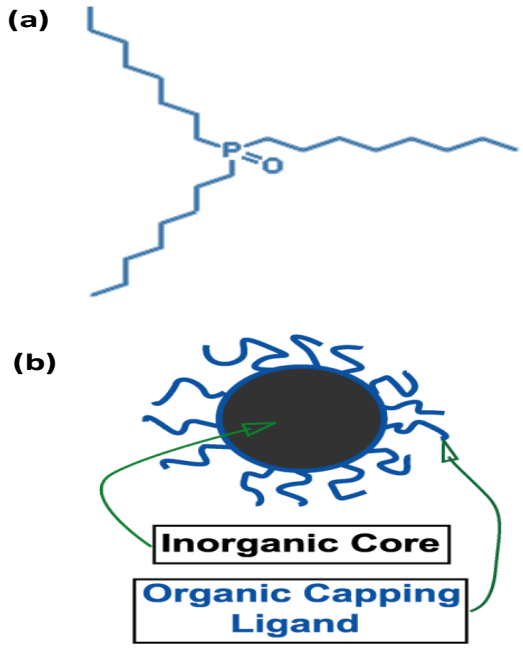

Fig. 2. (a) Structure of tri-n-octylphosphine oxide (TOPO) & (b) TOPO/TOP-capped CZTSSe nanoparticle.

TOP is known as a strong donor ligand, with both high polarity and polarizability contributing to its donor strength. Here, TOPO acts as an electron donor. TOPO binds to the acceptor sites in the nanoparticles through the lone pair on the oxygen as depicted in **Fig. 2(a)** providing a passivating shell to terminate growth, prevent agglomeration among particles, and its alkyl groups provide for excellent solubility in organic solvents such as toluene and hexane. TOP(alkylphosphines) co-ordination occurs with surface Se to form TOP-Se & are used as surfactants for more complete surface passivation. Both TOPO & TOP organic ligands are used as surfactants for regulating the particle size and for more complete surface passivation of the inorganic core CZTSSe nanoparticle (**Fig. 2(b)**).

CZTSSe Crystal Structure

In the past one decade, various research at theoretical level, have been done in order to envisage the formation mechanism and the physical properties of CZTSSecompounds. The formation of I_2–II–IV–VI_4 compounds like CZTSSe can be achieved froman II–VI semiconductor by sequential replacement of cations in which the octet rule isrespected and the total charge remains neutral (see **Fig. 3**) [**15**].

As evident from **Fig. 3**, binary compounds like CdTe adopt the cubic zinc blende structure in which there are two interpenetrating face-centered cubic crystals **[16]**. In the case of CIS a typical chalcopyrite structure, the ternary I–III–VI2 semiconductor alloys can be built by replacing the group II atom with two atoms of group I and III **[15-17]**. Thus, it is possible to split the ternary I–III–VI2 compound by replacing two atoms of group III with two atoms, respectively from group II and IV, forming a I2–II–IV–VI4 semiconductors in accordance with the octet rule.In fact, the amount of anions (chalcogens) introduced in the alloy depends on the amount of the cations and their valency: Cu(I), Sn(IV) and Zn(II).

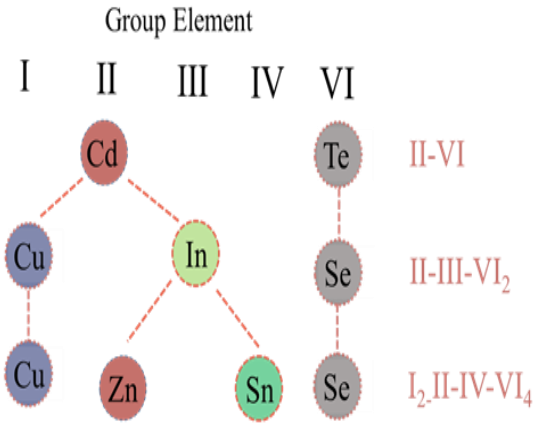

Fig. 3. Formation of stoichiometric I_2–II–IV–VI_4 compounds can be achieved by a sequential replacement of cations **[15]**.

As reported in the CZTSSe literature, the ratios of atomic percentages [Cu]/([Zn]+[Sn]) and[Zn]/[Sn] are often used to represent the composition of the cations in the alloy and for a stoichiometric material, both ratios are equal to one. However, it is observed that for CZTSSe-based devices, best solar cell efficiency were obtained for a composition ratio of ~0.8-0.9 for Cu/(Zn + Sn) and ~ 1.1-1.2 for Zn/Sn respectively [**13**].

$Cu_2ZnSn(S,Se)_4$ belongs to the I_2–II–IV–VI_4 quaternary material system with similar structure to that of ternary chalcopyrite material CuInSe2 (space group$\bar{I}$42d) (**Fig.4(a)**), in which one half of In atoms (group III) are replaced by Zn (group II) and other half by Sn atoms (group IV) respectively. It is known that $Cu_2ZnSn(S,Se)_4$ crystallizes in two primary crystalline structures known as kesterite (space group $\bar{I}$4) and stannite (space group $\bar{I}$42m) and are very similar. They both have cations located at tetrahedral sites but differ in the stacking arrangement of Cu and Zn atoms along the c-axis [**18, 19**]. The crystal structure and atomic arrangements for the kesterite and stannite structures are illustrated in **Fig. 4(b &c)**, respectively.

Theoretical studies have envisaged that the kesterite phase has slightly lower energy compared to the stannite phase and thus thermodynamically more stable as compared to its stannite counterpart [**20, 21**].

X-ray Diffraction Studies of CZTSSe-Based Nanoparticles

Since CZTSeS phase has a narrower region of phase stability as compared to chalcopyrites in which the device quality phase can be synthesized without any undesirable effect of secondary phases thus making single phase device quality CZTSeS synthesis more difficult and challenging. CZTSSe being a multicomponent semiconductor, there is always a possibility of co-existence of secondary phases along with CZTSSe main phase. Thus, phase purity analysis is of utmost importance in their XRD studies.

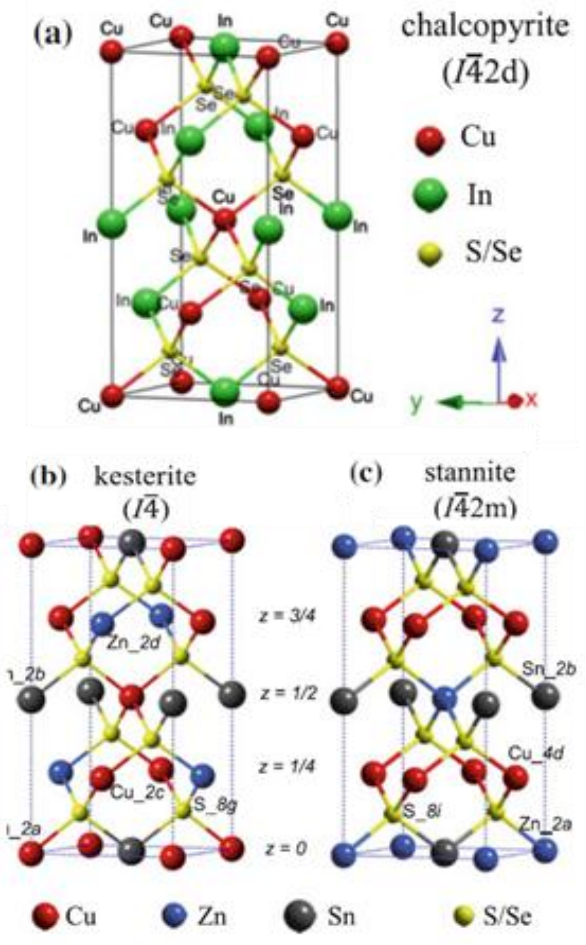

Fig. 4. Crystal structure representation of (a) chalcopyrite CI(S,Se); (b) kesterite $Cu_2ZnSn(S,Se)_4$ and (c) stannite $Cu_2ZnSn(S,Se)_4$ **[18]**.

Fig. 5(a-c) shows the XRD pattern of TOPO-capped CZTSe/CZTSSe/CZTS nanoparticles. The peaks of CZTSe originated from the following planes (112), (220), (312) upon indexing which is in agreement with others [**6**]. Although, the presence of XRD peak at 27.6° degree corresponding to (112) plane reveals the kesterite structure of CZTSSe [**6**]. However, since XRD peaks for Kesterite structure are similar to Stannite structure, it is difficult to distinguish between them unless other measurement techniques, such as Raman spectroscopy and neutron diffraction etc. are also employed. It is also quite likely that both kesterite and stannite structures co-exist simultaneously because there is not much of energy difference for these structures to achieve/attain a stable state [**20**]. As per Scherrer's equation, the crystallite size estimated from full width at half maximum (FWHM) of the (112) peak comes out to be in the range of 14-20 nm for CZTSSe-based nanocrystals respectively.

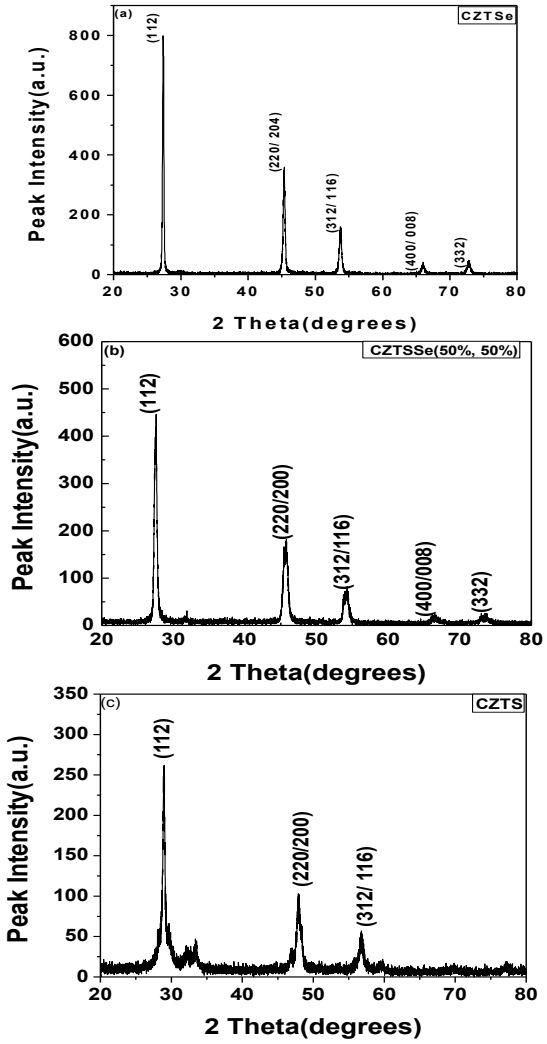

Fig. 5. X-ray Diffraction pattern of TOPO/TOP capped (a) CZTSe; (b) CZTSSe and (c) CZTS nanocrystals.

With increment in S content, i.e. for CZTSeS stoichiometric system (50%Se, 50%S), the XRD pattern (**Fig. 3(b)**) is similar to that of CZTSe (**Fig. 3(a)**) with no significant formation of any binary peaks related to metal sulphides or selenides. It is noteworthy to mention here that the highly intense (112) peak of CZTSSe mainly consists of an envelope of mainly two peaks corresponding to Se anion (lower angle side) and S anion (higher angle side) respectively. Moreover, from **Fig. 5(a-c),** it is quite evident that with increase in Se-content, [i.e. from CZTS (Se = 0 at. %) to CZTSSe (Se = S = 50 at.%) and to CZTSe (Se = 100 at.%, S = 0 at.%)], (112) peak intensity increases appreciably with concurrent decrease in FWHM values, thus implying enhancement in crystallinity and increment in crystallite size. These results are in good agreement with earlier reported ones [**6**, **23**].

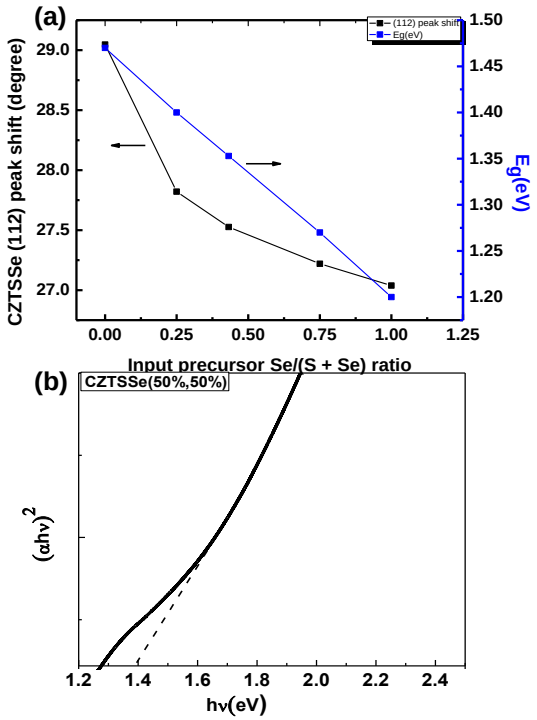

Fig. 6. (a) Relation between input precursor Se/(S + Se) ratio and shift in (112) peak position & E_g of CZTSSe; (b) Evaluation of band gap E_g by Tauc's formula for CZTSSe film deposited on glass substrate.

From **Fig. 6**, it is evident that with increase in input precursor (Se/(S + Se)) ratio, (112) peak position shifts toward lower diffraction angles. This can be attributed to the partial replacement of S by Se atoms in the lattice. As the S-content decreases, the larger Se atoms (1.98 Å) replace the smaller S atoms (1.84 Å) which creates disorder into the lattice thus, resulting in shifting of diffraction peaks toward lower angle [**7**, **19**]. As shown in **Fig. 6**, with increase in Se/(S + Se) ratio, the optical band gap decreases from 1.48 eV (CZTS) to 1.2 eV (CZTSe). Similar behavior has also been reported earlier [**24**]. The band gap values are calculated by plotting the square of alpha hυ vs. hυ and then by extrapolating the linear portion to the x-intercept where alpha being the absorption coefficient determined from the UV-VIS absorption spectra of CZTSSe thin film and hυ is the photon

energy. The CZTSSe nanocrystals display tunable band gaps in the range of 1.2 to 1.47 eV, indicating that the band gaps of the CZTSSe nanocrystals are mainly dependent on the Se/(S + Se) ratio. The size of nanocrystals decreases with increase in S or decrease in Se content and hence an increase in band gap. Here, it is important to note that for stoichiometric CZTSSe, the value of the band gap is found to be ~ 1.4 eV which is an ideal value for solar photoelectric conversion.

Fig. 7(a-c) shows the TEM images of colloidal TOPO-capped CZTSe/CZTSSe/CZTS nanocrystals. The as-synthesized CZTSe(100% Se) nanoparticles appear to be slightly polydispersed with polyhedral geometries and hexagonal phase formation having an average size of 20-30 nm with subgrain size ~5 nm. However, the agglomeration tendency decreases with decrease in Se content. For CZTSeS stoichiometric system (50%Se, 50%S), monodispersed, hexagonal-shaped, uniformly distributed nanocrystals (average size ~ 30 nm) were found. However, with further increment in S content i.e. for pure CZTS system, a marked change in morphology was observed as CZTS nanoparticles form monodispersed superstructures with a uniform three-dimensional flower-shaped configuration. As evident from **Fig. 2(c)**, these superstructures were built from crossed nanoflakes with thickness about 50 nm. Thus, distinct change in morphology was observed with variation in Se/S content.

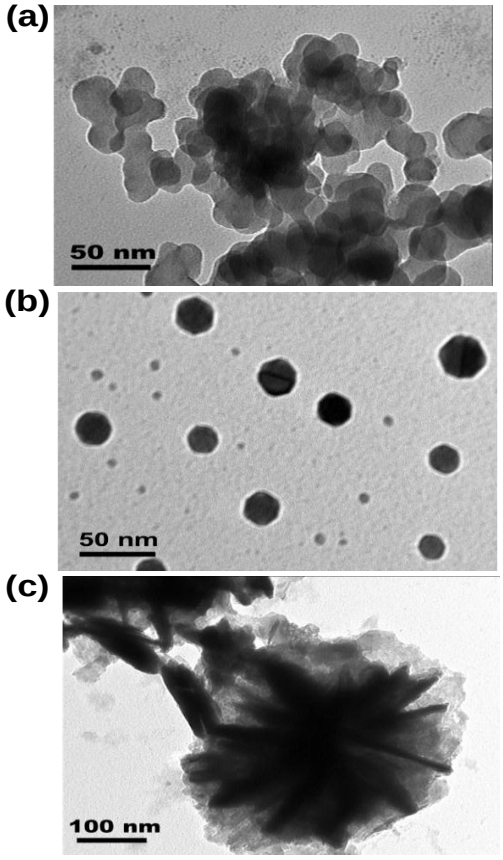

Fig. 7. TEM Micrographs of TOPO/TOP-capped (a) CZTSe; (b) CZTSSe and (c) CZTS nanoparticles.

From **Fig. 8**, I-V curves exhibits ~ mA current & shows photoresponse for CZTSSe-based devices with maximum (~ 10^{-3} A) and minimum (~ 10^{-4} A) current for CZTSSe and CZTS absorber layers respectively. The current voltage characteristics for CZTSSe-based devices can be further improved if (i)coating of CZTSSe based-inks by ink jet printing is done for uniform thin film deposition on substrates rather than by spin coating, drop-cast method [**25**] and (ii) there is a need to probe the interface between CIGSe-CdS better to further improve the junction properties [**26**]. The detailed studies are under-way.

Our solution-based synthesis approach has several advantages such as its adaptability for use with large-area substrates, high throughput and efficient materials utilization. The conventionally prepared CZTSSe-inks uses highly toxic and dangerously unstable hydrazine as one of its key components, which limits its use for low-cost and large-scale solar cell fabrication. Our preliminary results indicate that our environmentally benign ink approach is potentially viable for fabricating CZTSSe-based solar cells without resorting to highly toxic and flammable hydrazine and high temperature post-synthesis selenization/sulphur processes. Here, detrimental secondary phases have been avoided by careful tuning of the S/Se precursor ratios during our synthesis process.

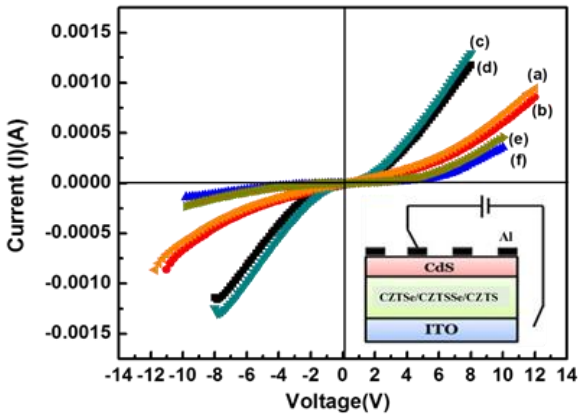

Fig. 8. Current (Photo & Dark)-Voltage (I-V) characteristics of (a & b) CZTSe; (c & d) CZTSSe and (e & f)CZTS. The inset shows the device structure.

Conclusion

Presently, one of the important p-type absorber $Cu_2ZnSn(Se_{1-x},S_x)_4$has reached a laboratory level efficiency of ~12% by non-vacuum process and has maintained a higher efficiency status as compared to its vacuum-based counterpart (efficiency ~ 9%). Although CZTSSe-based devices are beleaguered by complex phase diagram and narrow stoichiometry window; in addition, its interface properties with suitable hetero-junction partners (Mo, CdS & ZnO) needs to be understood better. However, despite these challenges, CZTSSe is the most promising material

synthesized using earth-abundant constituents by non-vacuum process technology, which has matured to a stage where it can be sincerely considered for commercialization. In this work, the authors have shown that polyhedral-shaped multicomponent chalcogenide nanocrystals (MCNs) of $Cu_2ZnSn(S_xSe_{1-x})_4$ having high monodispersity & uniform morphology can be successfully synthesized by the hot-injection method through careful tuning of the S and Se precursor reactivities using TOP/TOPO method. To the best of our knowledge, the combined usage of capping ligands TOP/TOPO in the synthesis of CZTSSe has been presented for the first time. A detailed probe on structural, optical and electrical properties shows sensitivity with increasing Se/(S + Se) ratio. From XRD studies, amongst the discussed set of chalcogenides, CZTSSe has been found to have acquired the most stable stannite/kesterite phase. TEM studies reveal better monodispersed polyhedral phase formation with faceted features for CZTSSe in comparison to the CZTSe and CZTS nanocrystallites where agglomeration tendency seems to be dominant and morphologies are different. The diameters of the CZTSSe-based nanocrystals mainly range from 14 to 20 nm. It is shown that the optical band gap of CZTSSe thin films can be tuned from 1.48 eV to 1.2 eV with concurrent augmentation in crystallinity with increase in Se/(S + Se) ratio. However, for stoichiometric CZTSSe and pure CZTSe films, the value of the band gap determined, lies in the range ~1.4-1.5 eV which approaches the optimum value for solar photoelectric conversion. The current-voltage characteristics of CZTSSe-based device exhibits ~ mA current and shows photoresponse as well. The synthesis of stoichiometric $Cu_2ZnSn(S_xSe_{1-x})_4$ nanocrystals reported herein now provides an avenue for probing the effect of Se inclusion in mixed-chalcogenide thin films and may lead to new routes for the fabrication of highly efficient CZTSSe nanocrystal PV devices without the need for post-deposition annealing in S/Se atmosphere.

Acknowledgements

The authors are grateful to Director (NPL) for his constant support and guidance. The authors gratefully acknowledge funding from the MNRE GAP 113532 project and are thankful to CSIR-India for TAP-SUN program.

Author's contributions

Conceived the plan: sns; Performed the experiments: pc, nv, js; Data analysis: sns, pc; Wrote the paper: sns (sns, pc, nj, js are the initials of authors). Authors have no competing financial interests.

References

1. Oleksak, R.P.; Flynn, B.T.; Schut, D.M.; Herman, G.S. *Physica Status Solidi (a)*. **2014,** *211*, 219.
2. Waldau, A.J.; *Solar Energy Mat. & Solar Cells*., **2011**, *95*, 1509.
3. Guo, Q;, Kim, S.J.; Kar, M.; Shafarman, W.N.; Birkmire, R.; Stach, E.A.; Agrawal, R.; Hillhouse, H.W; *Nano Letters*., **2008**, *8*, 2982.
4. Chawla, P.; Singh, S.; Sharma, S.N.; Beilstein J*; Nanotechnol.*, **2014,** *5*, 1235.
5. Dimitrievska, M.; Fairbrother, A.; Gunder, R.; Gurieva, G.; Xie, H.; Saucedo, E.; Perez-Rodriguez, A.; Izquierdo-Roca, V.; Schorr, S.; *Phys. Chem. Chem. Phys.*, **2016**, 18, 8692.
6. Singh, O.P.; Vijayan, N.; Sood, K.N.; Singh B.P.; Singh, V.N; *J. Alloys Compd.*, **2015**, *648*, 595.
7. Zeng, X.; Tai, K. F.; Zhang,T.; Ho, C.W.J.; Chen,X.; Huan,A.; Sum,T.C.; Wong, L. H; *Sol. Energ. Mater. Sol. Cells*, **2014**,*124*, 55.
8. Khadka, D. B.; Kim, S. Y.; Kim, J. H; *J. Phys. Chem. C*, **2016**, *120*, 4251.
9. Yang, K. J.; Son, D. H.; Sung, S. H.; Sim, J. H.; Kim, Y. I.; Park, S. N.; Jeon, D. H.; Kim, J.S.; Hwang, D. H.; Jeon, C.W.; Nam, D.; Cheong, H.; Kang J.K.; Kim D.H; *J. Mater. Chem. A*., **2016**,*4*, 10151.
10. Panthani, M.G.; Akhavan, V.; Goodfellow, B.; Schmidtke, J.P.; Dunn, L.; Dodabalapur, A.; Barbara, P.F.; Korgel, B. A. *J. Am. Chem. Soc.*, **2008**, *130*,16770.
11. Bari, R.H.; Patil, L.A.; Sonawane, P.S.; Mahanubhav, M.D.; Patil, V.R.; Khanna, P. K; *Mater. Lett.*, **2007**,*61*, 2058.
12. Bodnarchuk, M.; Kovalenko, M.V.; Pichler, S.; Fritz-Popovski, G.; Hesser, G.; Heiss, W.; *ACS Nano*, **2010**, *4*, 423.
13. Ou, K.L.;Fan, J.C.; Chen, J.K.; Huang, C.C.; Chen, L.Y.; Ho, J.H.; Chang, J.Y.; *J. Mater. Chem*., **2012**, *22*, 14667.
14. Riha, S. C.; Parkinson, B. A.; Prieto, A. L.; *J. Am. Chem. Soc.*, **2011**, *133*, 15272.
15. Giovanni Altamura. Development of CZTSSe thin films based solar cells". Material Chemistry. Universit_e Joseph-Fourier - Grenoble I, **2014**.
16. Ki,W.; Hillhouse,H. W.; *Adv. Energy Mater*., **2011**, *1*,732.
17. Triboulet,R.; Crestou,J.; Gasgnier,M.; *Journal of Crystal Growth*, **1994**, *143*, 40.
18. Das, S.; Mandal, K.C.; Bhattacharya, R.N.; Earth-Abundant $Cu_2ZnSn(S, Se)_4$ (CZTSSe) Solar Cells; Paranthaman, M.P.; et al.; (Eds.); Springer International Publishing:Switzerland, **2016**, pp. 25-74.
19. Mitzi, D.B.; Gunawan, O.; Todorov, T.K.; Wang, K.; Guha, S.; *Sol. Energy Mater. Sol. Cells*, **2011**, *95*, 1421.
20. Persson, C.; *J. Appl. Phys.*, **2010**, *107*, 053710.
21. Walsh, A.; Chen, S.; Wei, S.; Gong, X.; *Adv. Energy Mater.*, **2012**, *2*, 400.
22. Siebentritt, S.; Schorr, S.; *Progress in photovoltaics*, **2012**, *20*, 512.
23. Nagaoka,A.;Yoshino,K.;Taniguchi,H.;Taniyama,T.;Kakimoto,K.;Miyake,H.; *J. Cryst. Growth*, **2014**, *386*, 204.
24. He, J.; Sun, L.; Ding, N.; Kong, H.; Zuo, S.; Chen, S.;Chen,Y.;Yang,P.;Chu,J.; *J. Alloys Comp*., **2012**, *529*, 34.
25. Engberg, S.; Li, Z.; Lek, J.Y.; Lam, Y.M.; and Schou, J.; *RSC Adv.*, **2015**, *5*, 96593.
26. Chung ,Y. D.; Cho,D. H.; Choi,H. W.;Lee, K. S.;Ahn,B. J.; Song,J. H.; Kim, J.; *J. Kor. Phys. Soc*.,**2012**, *61*,1623.

